Available online at www.sciencedirect.com
SCIENCE DIRECT®
Journal of the European Ceramic Society 25 (2005) 481–487
www.elsevier.com/locate/jeurceramsoc

Ionic conductivities and phase transitions of lanthanide rare-earth substituted $La_2Mo_2O_9$

Dah-Shyang Tsai [a,*], Meng-Ju Hsieh [a], Jang-Chung Tseng [a], Hsin-Yi Lee [b]

[a] *Department of Chemical Engineering, National Taiwan University of Science and Technology, 43, Keelung Road, Sec. 4, Taipei 106, Taiwan*
[b] *National Synchrotron Radiation Research Center, 101 Hsin-Ann Road, Hsinchu Science Park, Hsinchu 300, Taiwan*

Received 18 December 2003; received in revised form 14 March 2004; accepted 21 March 2004
Available online 21 July 2004

Abstract

The ion conductivities and phase transitions of lanthanum molybdate ($La_2Mo_2O_9$) substituted with lanthanide rare-earths are investigated using impedance spectroscopy, dilatometry, and X-ray powder diffraction. Among the substituted $La_2Mo_2O_9$ of 10 mol% Ce, Nd, Sm, Gd, Dy, Er, Yb, the specimens containing Er, and Dy exhibit depressed α–β phase transformation and high conductivities. Their 700 °C conductivities are approximately five to seven times that of $La_2Mo_2O_9$, around 0.26 S cm^{-1}, comparable with those of (LaSr)(GaMg)O_3 and Gd-substituted CeO_2. Among the three compositions of 10 mol% Gd, Dy, Er showing depressed phase transition, Er- and Dy-substituted $La_2Mo_2O_9$ possess relatively low thermal expansion coefficient 11×10^{-6} K^{-1}, compared with that of the Gd-substituted $La_2Mo_2O_9$, 18×10^{-6} K^{-1}, which is near that of $La_2Mo_2O_9$. Hence, Dy and Er are valuable dopants in improving the $La_2Mo_2O_9$ properties. Across the lanthanide series, 10 mol%-substituted $La_2Mo_2O_9$ demonstrates systematic variations in the conductivity–temperature relation. Hysteresis phenomena in both of conductivity and thermal expansion are also observed in those compositions which display phase transition.

Keywords: $La_2Mo_2O_9$; Ionic conductivity; Thermal expansion; Phase transition; Transitions

1. Introduction

Lanthanum molybdate ($La_2Mo_2O_9$) which crystallizes at high temperatures in β-$SnWO_4$ structure of space group $P2_13$, is an oxygen ion conductor discovered by Lacorre et al.[1–3] The concept of lone-pair substitution has been proposed since a vacancy of oxygen ion size is generated when the Sn^{2+} ion possessing a lone pair of electrons is replaced by La^{3+} without the lone pair in the structure. This intrinsic vacancy facilitates oxygen ion diffusion and promises a high oxygen ion conductivity of the crystal.[4,5] $La_2Mo_2O_9$ crystal exhibits two polymorphs, a low-temperature monoclinic α-phase and a high-temperature cubic β-phase, with a reversible phase transition around 580 °C. The phase transition appears to be thermodynamically first order, it manifests itself as an endothermic event on heating and exothermic event on cooling in the differential thermal analysis curves. The structure of α-$La_2Mo_2O_9$ was described as a distorted cubic form of β-structure with $2 \times 3 \times 4$ superlattice. Its formation was assumed to be clustering of the oxygen vacancies which occurred in the order–disorder type of phase transition in stabilized zirconia.[2]

In its potential applications, such as electrolytes of solid oxide fuel cell, oxygen pumps, and oxygen sensors,[6–11] stabilization of the high temperature β-phase is important owing to the necessity to minimize stresses during the thermal cycles. Substitutions of Sr^{2+}, Ba^{2+}, K^{+}, Bi^{3+}, Ca^{2+} on the La site, S^{6+}, W^{6+}, Cr^{6+}, V^{5+} on the Mo site has been shown capable of reducing the phase transition temperature and stabilize the β-structure at a lower temperature.[4] For instance, the β-polymorph can be prepared in $La_2W_{2-x}Mo_xO_9$ for $x \geq 0.7$ at any cooling rate.[12] However, the suppression of phase transition often raises the low-temperature ion conductivity but not the high-temperature ion conductivity.[4] More detailed studies on substitutions of Ca^{2+}, Bi^{3+}, Pb^{2+} have also been carried out using the dielectric relaxation method.[13–16]

In this paper, we report variations in ion conductivities and thermal expansions in lanthanide rare-earth substituted $La_2Mo_2O_9$. The substitution of isovalent rare-earths has considerable influence on the properties of $La_2Mo_2O_9$. Some substitutions not only depress the phase transition,

* Corresponding author. Tel.: +886-2-2737-6618; fax: +886-2-2737-6644.
E-mail address: tsai@ch.ntust.edu.tw (D.-S. Tsai).

0955-2219/$ – see front matter © 2004 Elsevier Ltd. All rights reserved.
doi:10.1016/j.jeurceramsoc.2004.03.020

reduce the thermal expansion coefficient, but also enhance the high-temperature conductivity.

2. Experimental details

2.1. Specimen preparation

Stoichiometric amount of commercial MoO_3 (purity > 99.5%), La_2O_3 (purity > 99.9%) and calculated amount of rare-earth oxides CeO_2, Nd_2O_3, Sm_2O_3, Gd_2O_3, Dy_2O_3, Er_2O_3, and Yb_2O_3 (purity > 99.9%) were dried, weighed, mixed, and ball milled in a polyethylene jar with zirconia balls for fourteen hours. The powder was calcined at 880 °C for 10 h, and ball milled again. The powder was mixed with organic binders in the ball mill, dried, and sieved through a nylon sieve. Short rods and disks were pressed and sintered at 930 °C in air for 6 h. The relative densities of specimens used in impedance and dilatometric measurements were over 97%, measured by the Archimedes method.

2.2. Conductivity and thermal expansion coefficient measurement

Electrical resistance was measured by impedance spectroscopy technique using a Solartron S1260/1287 frequency response analyzer. The measurements were carried out over a frequency range of 1.0 Hz to 32 MHz. Each data point was recorded at a potential of 120 mV after 30 min of thermal stabilization in air. The measurement temperature range was between 300 and 800 °C, which was read from an inserted thermocouple near the specimen heated in a tubular furnace. The impedance measurements were performed at 5 or 10 °C interval in the temperature range that the α–β phase transition could occur. Thickness of the specimen was 15–24 mm, diameter 8–9 mm. Electrode contacts were formed on the parallel polished surfaces of the specimen by applying an unfluxed platinum paint (C3605P/S, Heraeus) and fired at 900 °C.

Thermal expansion coefficients of $La_2Mo_2O_9$ and rare-earth substituted $La_2Mo_2O_9$ were measured by dilatometry using a thermal mechanical analyzer (SETSYS-1750, SETARAM). The specimens used in dilatometry were disks of 1.7 mm thick and 8.0 mm in diameter. The ramping rate was 5 °C min^{-1} in both heating and cooling cycles from 300 to 800 °C. The phase transitions of substituted $La_2Mo_2O_9$ were checked by differential thermal analysis DTA (TGD7000H, Sinku-Riko). The calcined powder samples were sieved through a 90 μm sieve before the powder was subject to heating and cooling at a ramping rate of 5 °C min^{-1} in air.

2.3. X-ray diffraction analysis

X-ray diffraction patterns were recorded between 25 and 600 °C using the high resolution powder diffraction beamline 17B at the National Synchrotron Radiation Research Center, Hsinchu, Taiwan. The patterns were collected under the following conditions: wavelength 0.155 nm, angular range 20–60°, step size 0.02°, 2 s for a step of X-ray exposure, and 1 s for the detector rotation. The software UnitCell[17] is used in calculation of lattice parameter.

3. Results and discussion

3.1. Differential thermal analysis

Peak temperatures detected in DTA curves of 10 mol% lanthanide rare-earth substituted $La_2Mo_2O_9$ are listed in Table 1. Three compositions of $La_2Mo_2O_9$, $(La_{1.8}Ce_{0.2})Mo_2O_9$, and $(La_{1.8}Nd_{0.2})Mo_2O_9$ show reversible phase transitions with clear hysteresis during heating and cooling. The peak temperature difference between endothermic event (heating) and exothermic event (cooling) is about 20 °C for $La_2Mo_2O_9$ and $(La_{1.8}Ce_{0.2})Mo_2O_9$. This temperature difference is 40 °C for $(La_{1.8}Nd_{0.2})Mo_2O_9$. We didn't find relevant peaks in the DTA curves of $(La_{1.8}Sm_{0.2})Mo_2O_9$, $(La_{1.8}Gd_{0.2})Mo_2O_9$, $(La_{1.8}Dy_{0.2})Mo_2O_9$, $(La_{1.8}Er_{0.2})Mo_2O_9$, $(La_{1.8}Yb_{0.2})Mo_2O_9$. Nonetheless, as will be shown later, the α–β phase transition could reveal itself in a more subtle way for some compositions without clear endothermic and exothermic peaks.

3.2. Ion conductivities

Rare-earth substitutions exercise significant influences on the conductivity–temperature relation. The $La_2Mo_2O_9$ ceramics substituted with 10 mol% Ce, Nd, Sm, Gd, Dy, Er, Yb exhibit three types of temperature dependence. Figs. 1–4 illustrate these temperature dependences in Arrhenius plots of $\log(\sigma T)$ versus $1000/T$, σ and T are ion conductivity and temperature, respectively. A discontinuous jump in conductivity around the α → β transition temperature of $La_2Mo_2O_9$ is the feature common to the Arrhenius plots of $(La_{1.8}Ce_{0.2})Mo_2O_9$, $(La_{1.8}Nd_{0.2})Mo_2O_9$, $(La_{1.8}Sm_{0.2})O_9$, and $(La_{1.8}Yb_{0.2})Mo_2O_9$. The temperature dependence of $(La_{1.8}Ce_{0.2})Mo_2O_9$ conductivity is plotted along with that of $La_2Mo_2O_9$ in Fig. 1, since the temperature spans in phase transition of these two compositions are practically

Table 1
Peak temperatures in differential thermal analysis of lanthanide rare-earth substituted $La_2Mo_2O_9$ and the parent crystal $La_2Mo_2O_9$

Composition	Peak temperature (°C, heating)	Peak temperature (°C, cooling)
$(La_{1.8}Ce_{0.2})Mo_2O_9$	566	544
$(La_{1.8}Nd_{0.2})Mo_2O_9$	572	532
$La_2Mo_2O_9$	564	545

The heating and cooling rates are 5 °C min^{-1} in air. No peak related to α–β phase transition is detected in samples of 10 mol% Sm, Gd, Dy, Er, Yb.

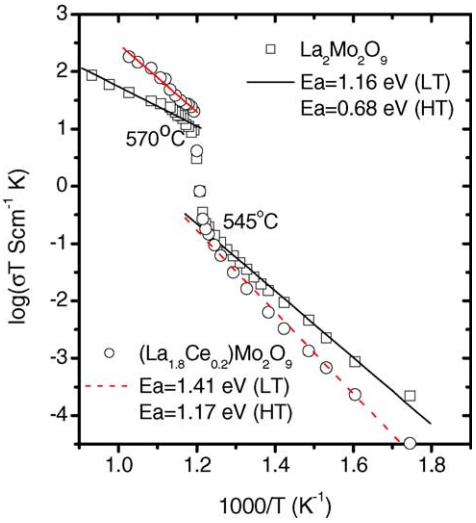

Fig. 1. Arrhenius plots of $\log(\sigma T)$ vs. $1000/T$ for $La_2Mo_2O_9$ and 10 mol% Ce-substituted $La_2Mo_2O_9$, σ is the ion conductivity.

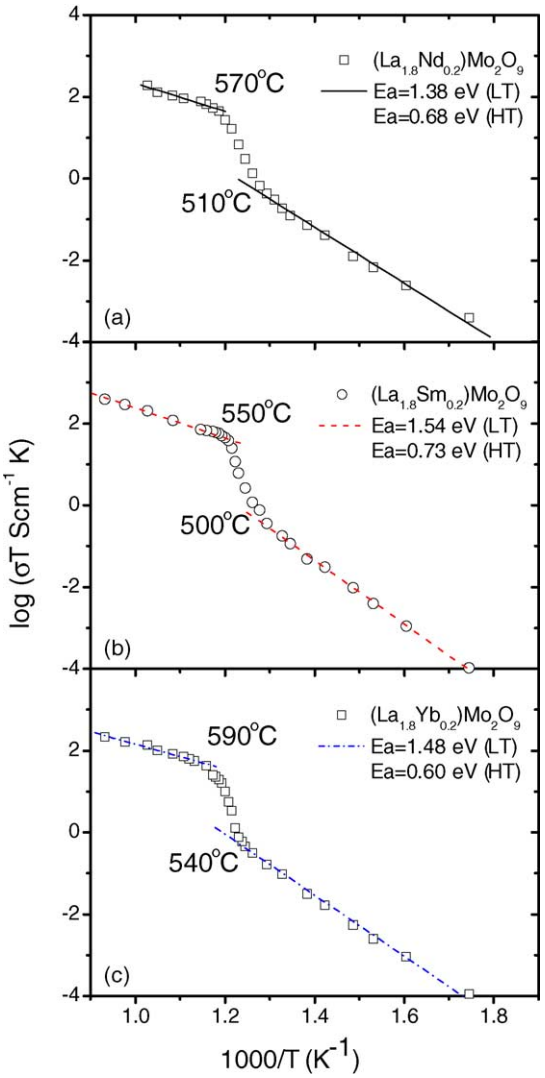

Fig. 2. Arrhenius plots of $\log(\sigma T)$ vs. $1000/T$ for 10 mol% (a) Nd-substituted, (b) Sm-substituted, (c) Yb-substituted $La_2Mo_2O_9$.

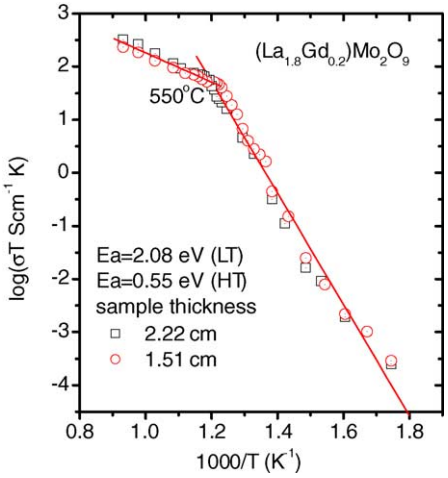

Fig. 3. Arrhenius plot of $\log(\sigma T)$ vs. $1000/T$ for 10 mol% Gd-substituted $La_2Mo_2O_9$.

the same, 545–570 °C. On the other hand, the temperature spans of $(La_{1.8}Nd_{0.2})Mo_2O_9$, $(La_{1.8}Sm_{0.2})Mo_2O_9$, and $(La_{1.8}Yb_{0.2})Mo_2O_9$ are much wider, 510–570 °C, 500–550 °C, and 540–590 °C, as indicated in Fig. 2.

Instead of a sudden jump, the Arrhenius plot of $(La_{1.8}Gd_{0.2})Mo_2O_9$ exhibits two segments of quite different temperature dependence connected at 550 °C (Fig. 3). The activation energy below 550 °C is 2.08 eV, while that above 550 °C 0.55 eV. Please note that the activation energies are correlated from experimental data of two 10 mol% Gd specimens of different thickness, one is 22.2 mm, the other 15.1 mm.

The temperature dependence of $(La_{1.8}Dy_{0.2})Mo_2O_9$ and $(La_{1.8}Er_{0.2})Mo_2O_9$ ion conductivities in 300–700 °C can be plotted in one straight line, illustrated in Fig. 4. Ion conductivities of these two compositions are similar in magnitude, with those of $(La_{1.8}Dy_{0.2})Mo_2O_9$ are somewhat higher in the high temperature range. Activation energy of

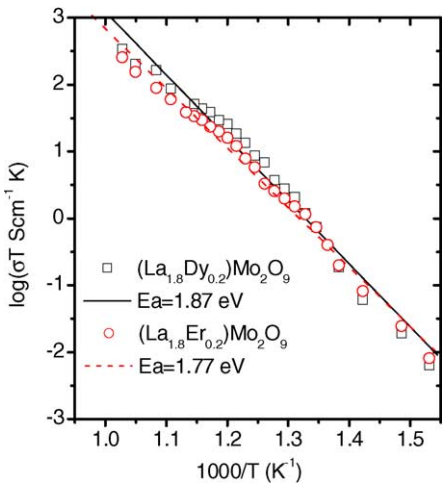

Fig. 4. Arrhenius plot of $\log(\sigma T)$ vs. $1000/T$ for 10 mol% Dy- and Er-substituted $La_2Mo_2O_9$.

Table 2
Activation energies E_a of the anion mobility in $La_2Mo_2O_9$ and those 10 mol% rare-earth substituted $La_2Mo_2O_9$

Composition	E_a of low-temperature phase (eV)	E_a of high-temperature phase (eV)
$La_2Mo_2O_9$	1.16	0.68
$(La_{1.8}Ce_{0.2})Mo_2O_9$	1.41	1.17
$(La_{1.8}Nd_{0.2})Mo_2O_9$	1.38	0.68
$(La_{1.8}Sm_{0.2})\ Mo_2O_9$	1.54	0.73
$(La_{1.8}Gd_{0.2})Mo_2O_9$[a]	2.08	0.55
$(La_{1.8}Dy_{0.2})Mo_2O_9$[b]	1.87	–
$(La_{1.8}Er_{0.2})Mo_2O_9$[b]	1.77	–
$(La_{1.8}Yb_{0.2})Mo_2O_9$	1.48	0.60

The activation energies are correlated from the plots of $\log(\sigma T)$ vs. $1000/T$.
[a] The temperature dependence of ion conductivity of this composition is correlated as two connected straight lines of different slope.
[b] The temperature dependence of ion conductivity of this composition is correlated in one straight line.

$(La_{1.8}Dy_{0.2})Mo_2O_9$ 1.87 eV is also slightly higher than that of $(La_{1.8}Er_{0.2})Mo_2O_9$ 1.77 eV. Nevertheless, the experimental data of $(La_{1.8}Dy_{0.2})Mo_2O_9$ deviate from a straight line more than those of $(La_{1.8}Er_{0.2})Mo_2O_9$. The deviation from the correlation line of $(La_{1.8}Dy_{0.2})Mo_2O_9$ is higher than that of $(La_{1.8}Er_{0.2})Mo_2O_9$, mainly because the experimental data of $(La_{1.8}Dy_{0.2})Mo_2O_9$ above 600 °C fall below its correlation line. It appears that the temperature dependence of $(La_{1.8}Dy_{0.2})Mo_2O_9$ in the high temperature region bears certain feature of $(La_{1.8}Gd_{0.2})Mo_2O_9$.

The activation energies of the oxygen vacancy mobility correlated from the slopes of Figs. 1–4 are listed in Table 2. For those compositions showing phase transition, the activation energies of less symmetric α phase are generally higher than those of β phase. The activation energies of vacancy mobility in α phase are between 1.16 and 1.54 eV. The activation energies in β phase are between 0.60 and 0.73 eV (except Ce), less than their counterparts in α phase. Apparently, the movement of oxygen vacancies in the high temperature β phase experience less obstruction than in the α phase.

Across the lanthanide series, the activation energy of low temperature region increases to a maximum value then decreases if the different temperature dependence in the high temperature region is ignored. The maximum activation energy 2.08 eV occurs at $(La_{1.8}Gd_{0.2})Mo_2O_9$. The enhancement of 10 mol% Nd, Sm on activation energy seems to be the consequence of tilting the slope of $\log(\sigma T)$ versus $1000/T$ at the α–β phase transition. For the three compositions of 10 mol% Gd, Dy, Er, the slopes at the phase transition are tilted so much that they are the same with the slopes in the low temperature region. In other words, substitutions of Gd, Dy, Er straighten out the sudden change in temperature dependence near the phase transition of $La_2Mo_2O_9$. Therefore, the activation energies of these three compositions are significantly higher than the rest.

The variation of ion conductivities with the Dy or Er content appears to follow the same trend. Fig. 5(a) depicts that

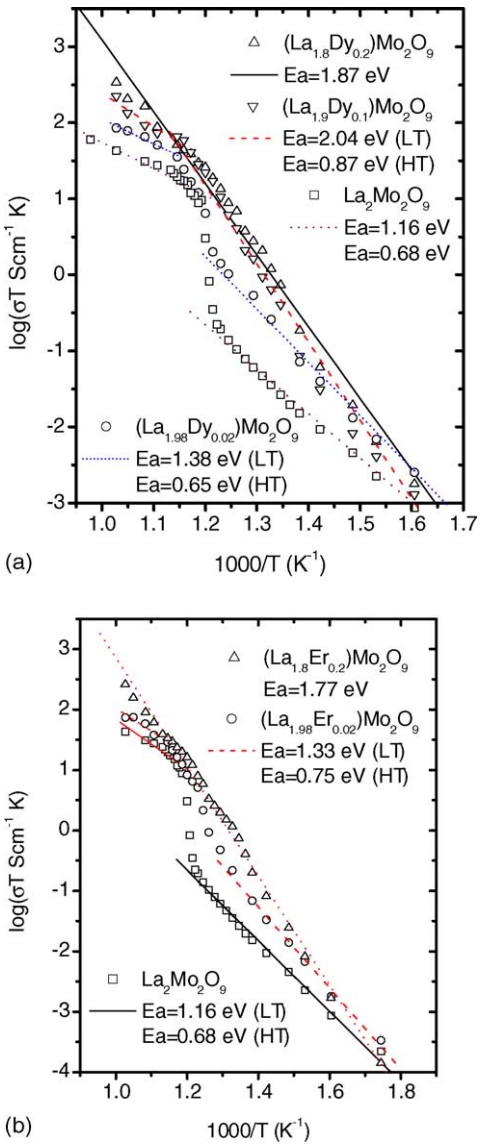

Fig. 5. (a) Arrhenius plot of $\log(\sigma T)$ vs. $1000/T$ for 0, 1, 5, and 10 mol% Dy-substituted $La_2Mo_2O_9$. (b) Arrhenius plot of $\log(\sigma T)$ vs. $1000/T$ for 0, 1, and 10 mol% Er-substituted $La_2Mo_2O_9$.

the Arrhenius plot evolves with 0, 1, 5 and 10 mol% Dy. Upon 1 mol% Dy substitution, the slope at phase transition becomes tilted, similar with those of 10 mol% Nd and Sm substitution. If the Dy content level increases to 5 mol%, the Arrhenius plot of $(La_{1.9}Dy_{0.1})Mo_2O_9$ develops into two linear segments, similar to that of 10 mol% Gd. Variation of activation energy with the Dy content in the low temperature region is as follows, 1.16 eV (0 mol%), 1.38 eV (1 mol%), 2.04 eV (5 mol%), 1.87 eV (10 mol%). Fig. 5(b) presents how the Arrhenius plot varies with 0, 1 and 10 mol% Er. The Er substitution is very effective in straightening out the jump at phase transition. The 1 mol% Er addition tilts the slope at phase transition and raises the activation energy from 1.16 to 1.33 eV. Further increasing the Er content to 5–10 mol%,

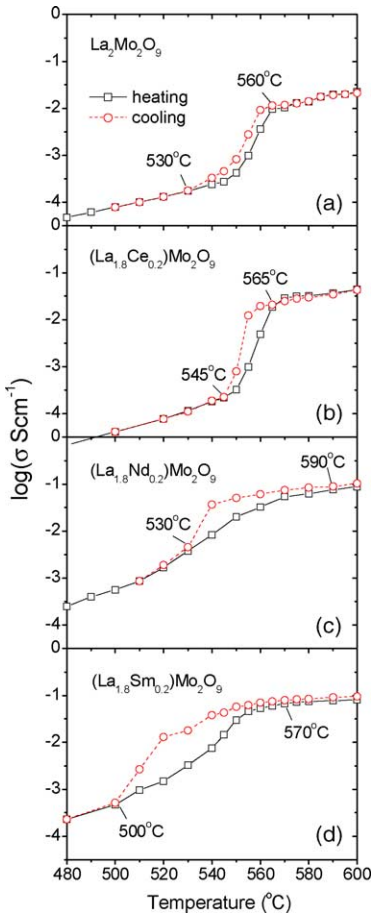

Fig. 6. Hysteresis of ion conductivity while heating and cooling of (a) $La_2Mo_2O_9$-substituted, (b) 10 mol% Ce-substituted, (c) 10 mol% Nd-substituted, (d) 10 mol% Sm-substituted $La_2Mo_2O_9$.

the relation between $\log(\sigma T)$ and $1000/T$ turns into a straight line.

Hysteresis in the α–β phase transition is a feature common to all compositions which exhibit discontinuous jumps in conductivities, indicated in Fig. 6. Similar to other types of hysteresis, on cooling, the jump occurs at a somewhat lower temperature compared with the heating cycle. Compositions of $La_2Mo_2O_9$ and $(La_{1.8}Ce_{0.2})Mo_2O_9$ having abrupt changes during phase transitions also display narrow hysteresis loops. On the other hand, $(La_{1.8}Nd_{0.2})Mo_2O_9$ and $(La_{1.8}Sm_{0.2})Mo_2O_9$ having sluggish changes in heating exhibit larger hysteresis loops. The hysteresis loop of $(La_{1.8}Yb_{0.2})Mo_2O_9$, not present in Fig. 6, is similar to those of $(La_{1.8}Nd_{0.2})Mo_2O_9$ and $(La_{1.8}Sm_{0.2})Mo_2O_9$. Hysteresis phenomena vanish in $(La_{1.8}Gd_{0.2})Mo_2O_9$, $(La_{1.8}Dy_{0.2})Mo_2O_9$, and $(La_{1.8}Er_{0.2})Mo_2O_9$.

The high-temperature conductivities of rare-earth substituted $La_2Mo_2O_9$ after the phase transition are similar in magnitude. Among the four compositions of 10 mol% Ce, Nd, Sm, Yb, the ion conductivities of Ce, Nd, Sm at 700 °C are around 0.19 S cm^{-1}, that of Yb is somewhat lower 0.14 S cm^{-1}. These conductivities are higher than that

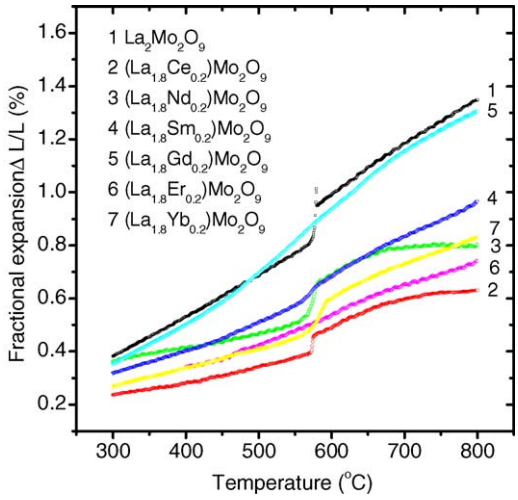

Fig. 7. Fractional expansions of $La_2Mo_2O_9$ and 10 mol% rare-earth substituted $La_2Mo_2O_9$ on heating. The heating rate is 5 °C min^{-1}.

of $La_2Mo_2O_9$, 0.044 S cm^{-1}. The 700 °C conductivity of $(La_{1.8}Gd_{0.2})Mo_2O_9$ is about 0.19 S cm^{-1}, which is comparable to those of 10 mol% Ce, Nd, Sm. The high-temperature conductivities of 10 mol% Dy and Er are higher. The 700 °C conductivity of $(La_{1.8}Dy_{0.2})Mo_2O_9$ is 0.35 S cm^{-1}, and that of $(La_{1.8}Er_{0.2})Mo_2O_9$ 0.26 S cm^{-1}. The 700 °C conductivity of $(La_{1.8}Dy_{0.2})Mo_2O_9$ is the highest measured value among those of 10 mol% lanthanide substituted $La_2Mo_2O_9$.

3.3. Thermal expansion coefficient

Fractional expansions of $La_2Mo_2O_9$ and the rare-earth substituted $La_2Mo_2O_9$ ceramics in the heating cycle are plotted in Fig. 7. Those compositions which exhibit clear jumps in conductivities also display sudden changes in the linear expansions at the α–β phase transition. Similarly, near the phase transition, fractional expansions $La_2Mo_2O_9$ and $(La_{1.8}Ce_{0.2})Mo_2O_9$ increase more steeply than those of $(La_{1.8}Nd_{0.2})Mo_2O_9$, $(La_{1.8}Sm_{0.2})Mo_2O_9$, and $(La_{1.8}Yb_{0.2})Mo_2O_9$. During the phase transition of $La_2Mo_2O_9$, the specimen expands 0.15% at 575 °C in the heating cycle, and contracts 0.12% at 559 °C in the cooling cycle. In the case of $(La_{1.8}Ce_{0.2})Mo_2O_9$, the fractional change at phase transition is about half that of $La_2Mo_2O_9$, 0.06% at 573 °C in heating and 545 °C in cooling. The phase transitions in linear dimension changes of $(La_{1.8}Nd_{0.2})Mo_2O_9$, $(La_{1.8}Sm_{0.2})Mo_2O_9$, and $(La_{1.8}Yb_{0.2})Mo_2O_9$ occur over a larger temperature region. For example, $(La_{1.8}Nd_{0.2})Mo_2O_9$ expands about 0.16% near 561 °C and contracts 0.11% near 522 °C.

In general, the fractional expansions of 10 mol% lanthanide rare-earth substitutions are less than that of the parent compound $La_2Mo_2O_9$. The fractional expansions of $(La_{1.8}Gd_{0.2})Mo_2O_9$ are quite high, near those of $La_2Mo_2O_9$. The experimental data of these two compositions are in such a close proximity that the $(La_{1.8}Gd_{0.2})Mo_2O_9$ curve looks

like a straightened line of $La_2Mo_2O_9$ curve. Although two segments in fractional expansion of $(La_{1.8}Gd_{0.2})Mo_2O_9$ are distinguishable, identification of the switching point is difficult. The switching from low-temperature expansion to high-temperature expansion occurs over a vast temperature region, at least 150 °C. The fractional expansions of $(La_{1.8}Er_{0.2})Mo_2O_9$ are much less than that of $(La_{1.8}Gd_{0.2})Mo_2O_9$ in magnitude. The relation between fractional expansion and temperature for $(La_{1.8}Er_{0.2})Mo_2O_9$ appears to be linear.

The thermal expansion coefficient TEC of α-$La_2Mo_2O_9$ is $14.7 \times 10^{-6}\,C^{-1}$, that of β-$La_2Mo_2O_9$ is higher, $18.1 \times 10^{-6}\,C^{-1}$. Substitutions of rare-earths reduce the values of TEC, except Gd. TEC of $(La_{1.8}Gd_{0.2})Mo_2O_9$ is $15.8 \times 10^{-6}\,C^{-1}$ in 50–555 °C, and $19.0 \times 10^{-6}\,C^{-1}$ in 555–800 °C. TEC of $(La_{1.8}Er_{0.2})Mo_2O_9$ is low, $10.6 \times 10^{-6}\,C^{-1}$. Fig. 7 also points out that no systematic reduction in the TEC value can be found owing to the size reduction in substitutional ions. The expectation of reduction in TEC arises from the well-known lanthanide contraction because the $La_2Mo_2O_9$ lattice is supposed to shrink gradually when the lanthanum ion is replaced with ions of decreasing size.

3.4. X-ray diffraction using synchrotron source

The α-polymorph has been described as a distorted monoclinic form of the cubic β-$La_2Mo_2O_9$. The distortion is quite small, and causes a number of X-ray reflections of β-polymorph, such as (1 1 1) (2 1 0) (2 1 1) (3 2 1), to split into doublets or triplets.[2] However, the X-ray diffraction patterns of $(La_{1.8}Gd_{0.2})Mo_2O_9$ do not indicate such doublets

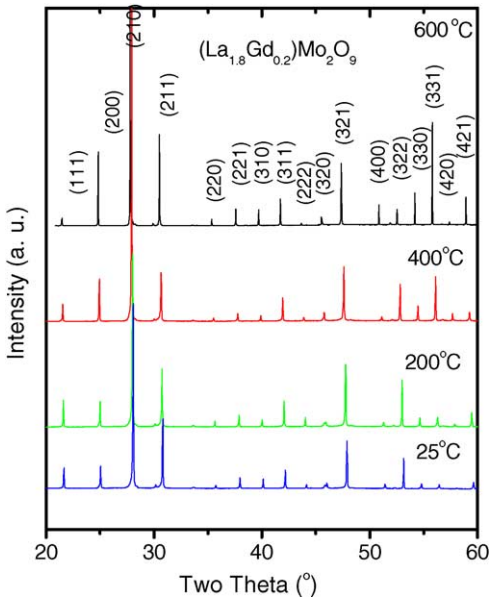

Fig. 8. X-ray diffraction patterns (synchrotron radiation) of 10 mol% Gd substituted $La_2Mo_2O_9$ at 600, 400, 200, and 25 °C. The intensity of (3 3 1) reflection is relatively low at 200 and 25 °C owing to different samples being used at 400 and 600 °C, which could have certain preferential orientation effects.

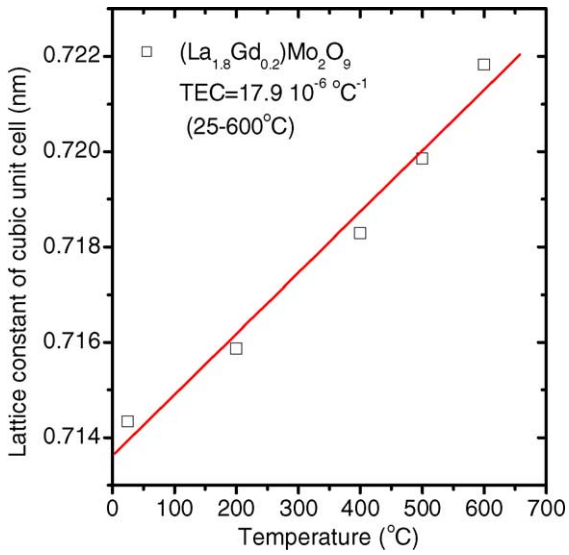

Fig. 9. Thermal evolution in cell parameter *a* of 10 mol% Gd susbstituted $La_2Mo_2O_9$.

or triplets at 25, 200, 400 and 600 °C (Fig. 8). The only exception is the reflection (3 2 0) which splits into a doublet below 400 °C. This result along with the clean X-ray diffraction patterns of $(La_{1.8}Dy_{0.2})Mo_2O_9$ and $(La_{1.8}Er_{0.2})Mo_2O_9$ suggest that the three compositions of 10 mol% Gd, Dy, Er are stabilized β-polymorph.

Fig. 9 shows the plot of lattice constant of cubic unit cell of $(La_{1.8}Gd_{0.2})Mo_2O_9$ versus temperature. At 600 °C, the fitted lattice parameter of $(La_{1.8}Gd_{0.2})Mo_2O_9$ $a = 0.72183$ nm, higher than that of $La_2Mo_2O_9$ is 0.72240 nm. The observation of decrease in the cell volume and increase in ion conductivity on Gd substitution is consistent with the report of Lacorre.[18] The linear thermal expansion coefficient calculated from Fig. 9 is $17.9 \times 10^{-6}\,°C^{-1}$, which is consistent with the TEC value measured by dilatometry, $18.1 \times 10^{-6}\,°C^{-1}$.

4. Summary

Ion conductivity and thermal expansion coefficient are two crucial properties of solid state ionics in their applications. The two properties of $La_2Mo_2O_9$ can be enhanced in a positive direction by substituting with lanthanide rare-earths. In this study, we have examined seven rare-earths, Ce, Nd, Sm, Gd, Dy, Er, Yb. On the effect of discouraging the α–β phase transition of $La_2Mo_2O_9$, 10 mol% Gd, Dy, Er can eliminate the sudden jumps and hysteresis in both ion conductivity and thermal expansion at phase transition. Across the lanthanide series, the high-temperature ion conductivity first increases, reaches a maximum value around Dy, then decreases. Such an increase-then-decrease variation with atomic number cannot be found in thermal expansion coefficient. Among the three compositions of 10 mol% Gd, Dy, Er, samples of Dy and Er have the benefit of low

thermal expansion coefficient, around $10^{-5}\,^{\circ}C^{-1}$. Although the phase transition of 10 mol% Gd is largely depressed, its thermal expansion coefficient is high, $18.1 \times 10^{-6}\,^{\circ}C^{-1}$, similar to that of the parent crystal.

Investigation on the ion conductivity of 10 mol% rare-earth substituted $La_2Mo_2O_9$ reveals interesting and systematic variations with the atomic number of rare-earth. The substitution of Nd or Sm decreases the slope at the phase transition in Arrhenius plot. The substitution of Gd, Dy, or Er decreases the slope at the phase transition so much that the phase transition vanishes. The less abrupt jump in conductivity at the phase transition emerges again on Yb substitution. The study on the dependence of ion conductivity on the Dy and the Er content indicates its variation is similar to the influence of atomic number. The Arrhenius plot of 1 mol% Dy or Er looks similar to that of 10 mol% Nd or Sm. The Arrhenius plot of 5 mol% Dy appears similar with that of 10 mol% Gd. It can be concluded that Dy and Er are the most effective rare-earth elements in this study.

Acknowledgements

The authors are grateful to National Science Council of Taiwan for the financial support through Grant No. NSC 92-NU-7-011-001.

References

1. Lacorre, Ph., The LPS concept, a new way to look at anionic conductors. *Solid State Sci.* 2000, **2**, 755–758.
2. Goutenoire, F., Isnard, O., Retoux, R. and Lacorre, Ph., Crystal structure of $La_2Mo_2O_9$, a new fast oxide-ion conductor. *Chem. Mater.* 2000, **12**, 2575–2580.
3. Lacorre, Ph., Goutenoire, F., Bohnke, O., Retoux, R. and Laligant, Y., Designing fast oxide-ion conductors based on $La_2Mo_2O_9$. *Nature* 2000, **404**, 856–858.
4. Goutenoire, F., Isnard, O., Suard, E., Bohnke, O., Laligant, Y., Retoux, R. *et al.*, Structural and transport characteristics of the LAMOX family of fast oxide-ion conductors, based on lanthanum molybdenum oxide $La_2Mo_2O_9$. *J. Mater. Chem.* 2001, **11**, 119–124.
5. Skinner, S. J. and Kilner, J. A., Oxygen ion conductors. *Mater. Today* 2003, **6**, 30–37.
6. Haile, S. M., Fuel cell materials and components. *Acta Mater.* 2003, **51**, 5981–6000.
7. Minh, N. Q., Ceramic fuel cells. *J. Am. Ceram. Soc.* 1993, **76**, 563–588.
8. Kilner, J. A., Fast oxygen transport in acceptor doped oxides. *Solid State Ionics* 2000, **129**, 13–23.
9. Goodenough, J. B., Ceramic solid electrolytes. *Solid State Ionics* 1997, **94**, 17–25.
10. Norby, T., Fast oxygen ion conductors. *J. Mater. Chem.* 2001, **11**, 11–18.
11. Boivin, J. C. and Mairesse, G., Recent material developments in fast oxide ion conductors. *Chem. Mater.* 1998, **10**, 2870–2888.
12. Collado, J. A., Aranda, M. A. G., Cabeza, A., Olivera-Pastor, P. and Bruque, S., Synthesis, structures, and thermal expansion of the $La_2W_{2-x}Mo_xO_9$ series. *J. Solid State Chem.* 2002, **167**, 80–85.
13. Zhang, G. G., Fang, Q. F., Wang, X. P. and Yi, Z. G., AC impedance and dielectric relaxation study on the effects of the excess Pb introduction in $La_2Mo_2O_9$ oxide ion conductors. *Phys. Stat. Sol.* 2003, **199**, 329–334.
14. Yi, Z. G., Fang, Q. F., Wang, X. P. and Zhang, G. G., Dielectric relaxation studies on the submicron crystalline $La_2Mo_2O_9$ oxide ion conductors. *Solid State Ionics* 2003, **160**, 117–124.
15. Wang, X. P., Fang, Q. F., Li, Z. S., Zhang, G. G. and Yi, Z. G., Dielectric relaxation studies of Bi-doping effects on the oxygen-ion diffusion in $La_{2-x}Bi_xMo_2O_9$ oxide ion conductors. *Appl. Phys. Lett.* 2002, **81**, 3434–3436.
16. Wang, X. P. and Fang, Q. F., Effects of Ca doping on the oxygen ion diffusion and phase transition in oxide ion conductor $La_2Mo_2O_9$. *Solid State Ionics* 2002, **146**, 185–193.
17. Holland, T. J. B. and Redfern, S. A. T., Unit cell refinement from powder diffraction data: the use of regression diagnostic. *Mineral. Mag.* 1997, **61**, 65–77.
18. Georges, S., Goutenoire, F., Altorfer, F., Sheptyakov, D., Fauth, F., Suard, E. *et al.*, Thermal, structural and transport properties of the fast oxide-ion conductors $La_{2-x}R_xMo_2O_9$ (R = Nd, Gd, Y). *Solid State Ionics* 2003, **161**, 231–241.